Assessing Tracheal Health Using Optical Metabolic Imaging and Optical Coherence Tomography

by

Daniel Ari Gil

Thesis
Submitted to the Faculty of the
Graduate School of Vanderbilt University
in partial fulfillment of the requirements
for the degree of

MASTER OF SCIENCE
in
Biomedical Engineering
December, 2016
Nashville, Tennessee

Approved:

Melissa C. Skala, Ph.D.

Yuankai (Kenny) Tao, Ph.D.

ACKNOWLEDGEMENTS

I'd like to thank Joe Sharick for his significant efforts on these studies and Ute Gamm, Michael Choma, and Melissa Skala for their useful discussions throughout. Additionally, I would like to thank Kristin Poole O'Grady and Chetan Patil for the time they spent training me on optical coherence tomography instrumentation and theory.

TABLE OF CONTENTS

Page

LIST OF FIGURES

Figure Page

CHAPTER I

INTRODUCTION

Increasing burden of respiratory disease

Respiratory diseases represent a significant healthcare and economic burden worldwide, with a global prevalence higher than both cancer and cardiovascular disease (2015 estimate: 532 million vs. 90 million and 423 million, respectively) leading to the third most deaths (2015 estimate: 7.6 million vs. 8.7 million and 17.9 million, respectively)[1–3]. While progress has been made in reducing the effect and incidence of respiratory diseases in developed countries, the trend towards urbanization in developing countries has led to increased prevalence of many chronic respiratory diseases, such as asthma and chronic obstructive pulmonary disease (COPD), due to increasing exposure to indoor and outdoor pollutants and tobacco consumption[4]. Despite effective therapies for both COPD and asthma, many patients have low qualities-of-life because of poorly controlled symptoms[5,6]. Overcrowding in cities has also lead to increased tuberculosis (TB) incidence and continued high levels of mortality from acute respiratory infections, which is the leading cause of death for children under 5 years old worldwide[7,8]. While treatments currently exist to treat bacterial respiratory infections, multidrug-resistant bacteria, including multidrug-resistant strains of the TB bacterium, will represent a significant challenge in the future due to the lack of effective treatments and the risk of transmission among at-risk populations (i.e., immunocompromised, the young, and the elderly)[9,10]. Overall, respiratory diseases are a significant cause of mortality, morbidity, and reduced quality-of-life around the world that will only increase in the coming decades[1].

New therapies are required to improve the mortality and morbidity of respiratory diseases, but, unlike other diseases, respiratory medicine has seen fewer new classes of safe and effective

drugs developed over the last 40 years[11]. Fewer drug candidates for respiratory diseases are developed and only 3% of these drugs reach market, compared to 6-14% for other diseases, leading to greater costs and longer durations for respiratory drug development than other areas[11]. Failure late in the drug development process due to unexpected adverse effects or toxicity occur in approximately 33% of potential new therapeutics, and those that fail at this stage are the most expensive[12]. Reducing the attrition rate of new respiratory drugs, especially late stage attrition, would have a significant impact on drug development cost[13]. This breakdown in the respiratory drug development pipeline is likely due to a number of factors, including a poor understanding of respiratory disease mechanisms, poor preclinical models for testing treatments, and the difficulty of developing inhaled drugs[11].

The National Research Council Report on Toxicity in the 21st Century specifically addresses the need to improve early stage toxicity screening to be more predictive of human safety[14]. Historically, animal studies using mice or rats have been the gold standard to predict future human toxicity, but animal studies are expensive, time-intensive, low-throughput, and, due to interspecies differences, not necessarily predictive of human response[15,16]. *In vitro* cytotoxicity assays using cell monolayers, while convenient, do not effectively predict human toxicity due to their simplicity[17]. Recent advances in 3D *in vitro* culture methods that better recapitulate the *in vivo* environment such as cultured primary tissue, organoids, microfluidic devices, and lungs-on-a-chip have drastically increased the complexity and physiological relevance of these models[18–21]. Extracting as much data as possible from these *in vitro* models is vital to understand the mechanism of action of new drugs and screen for toxicity and efficacy across a wide range of doses, and has been shown to lead to reduced false positive and false negative rates[22]. However, while *in vitro*

model technology has seen recent advances, the assays used to evaluate the effects of drug toxicity have not dramatically changed over the last 10 years[23].

We believe that leveraging advances in optical microscopy will provide the tools necessary to improve the respiratory drug development pipeline in three ways: 1. improve our understanding of the underlying disease mechanism, 2. provide detailed information about the functional response of preclinical models to drugs, and 3. facilitate repeated measurements of *in vitro* models. Specifically, using more relevant *in vitro* respiratory models with novel microscopic assays may allow researchers to identify issues related to toxicity early in the discovery process, when it is still possible to optimize desirable drug attributes and minimize potential adverse effects. This approach would enable researchers to select drug candidates for preclinical safety and efficacy trials with the highest probability of success.

Improved assays for respiratory drug development

The respiratory system consists of the trachea, bronchi, and the lungs. Within the lungs, specialized structures, the alveoli, handle gas exchange between the inhaled air and the red blood cells passing through the capillary network of the lungs. During normal respiration, the respiratory system is exposed to external agents such as bacteria, viruses, fungi, allergens, and toxins in the form of pollutants or tobacco smoke. These agents encounter the epithelial cells that lines the respiratory tract and are caught in mucus to be transported away from the lungs by the motility of ciliated epithelia cells[24]. Dysfunction of ciliary motility leading to impaired mucociliary clearance, such as in primary ciliary dyskinesia and cystic fibrosis, is known to lead to chronic respiratory infections and significant morbidity and mortality[25]. In addition, these external agents cause airway epithelial cells to initiate an inflammatory response. Repeated airway inflammation has been

implicated in asthma and COPD[26]. While airway epithelial cells clearly play a central role in the pathogenesis of most respiratory diseases, additional cell types such as airway smooth muscle cells, fibroblasts, and immune cells also play a significant role[27]. Novel *in vitro* models of the healthy and diseased respiratory system are increasingly complex, containing multiple cell types in a 3D environment, and evaluating these complex *in vitro* models will involve developing replacements for current assays.

Current assays were designed to be applied to cell monolayers and integrate a readout over the entire cell population in a dish, losing all information about the response of different cell types and the interactions of cells with other cells and cells with the microenvironment[28]. Also, many assays that give functional readouts on cellular metabolism or toxicity involve non-vital dyes or non-physiological media such as DMSO, requiring the sacrifice of the cell population at every time point[29,30]. Ideally, new assays would be able to resolve the time-dependent response of cells to compounds in a more physiological environment while being sensitive to early cell injury and different pathways of drug toxicity. Label-free assays based on light microscopy fit these requirements as they could be performed without the sacrifice of cells at specific time points, allowing early and late assessment of toxicological dynamics in the same 3D model. Additionally, microscopy offers the ability to understand the spatial relation between cell types and how that affects drug bioavailability, toxicity, and cellular metabolism. Thus, there is a need to develop new label-free microscopy techniques that can evaluate drug response and potential toxicity in *in vitro* respiratory models and models of off-target organs such as the heart, brain, and liver[31].

Standard light microscopy of cells is noninvasive and can measure changes in cell morphology. Researchers have also explored using digital holographic microscopy as a label-free assay, which works well for monolayers, but cannot be extended to 3D cultures[32]. Novel toxicity

assays based on organoid/spheroid morphology or multiple fluorophores have been shown to agree with known cytotoxicity of drugs, but give limited about the pathways affected by drugs that lead to toxicity, require the sacrifice of cells, or integrate the response over the entire population of cells within a dish[33–35]. Because many of the current toxicity assays measure the result of significant changes in cellular metabolism (i.e., the result of apoptosis or necrosis), we believe that non-destructive assays based on microscopy sensitive to slight alterations in the metabolism of each cell in a dish would be beneficial.

Optical imaging of cellular metabolism as a biomarker of toxicity

Many compounds lead to cellular toxicity either by directly or indirectly affecting energy production pathways within the cell[36]. Mitochondria are the cellular organelles whose dominant function is to produce more than 90% of the cell's energy in the form of adenosine triphosphate (ATP) through oxidative phosphorylation. At first, impairment in mitochondrial activity causes cells to rely more on glycolysis, but when mitochondrial metabolic capacity becomes insufficient, cells either succumb to necrosis or apoptosis. Optical metabolic imaging (OMI) is a technique sensitive to cellular metabolism that has had recent success in cancer biology in assessing the cytotoxic effects of cancer therapeutics, but the potential of OMI in respiratory biology and drug development has only recently started to be explored[37,38]. OMI quantitatively assesses the metabolic state of cells by measuring the fluorescence intensities of endogenous metabolic coenzymes nicotinamide adenine dinucleotide (NADH) and flavin adenin dinucelotide (FAD)[39]. NADH and FAD play a role in multiple metabolic pathways within the cell including oxidative phosphorylation, fatty acid oxidation, and glycolysis. Both fluorophores have well established fluorescence spectra with excitation maxima of 350nm and 435nm and emission maxima of 460nm

and 535nm, respectively. NADH fluorescence is typically more intense due to the higher quantum yield compared to FAD. Due to their involvement in cellular metabolism and unique fluorescence signatures, both coenzymes act as indicators of physiological change within a cell. A useful parameter is the optical redox ratio defined as the intensity of NADH divided by the intensity of FAD, which is sensitive to the relative amounts of electron donors and acceptors within a cell and has been shown to separate cells responding to cytotoxic drugs from non-responsive cells[40,41]. Understanding how OMI can be applied to respiratory models of disease and drug screening may provide an important tool for improving preclinical results and translation of new drugs to the clinic. OMI is attractive for assessing toxicity in drug development assays as it requires no dyes or labels, allowing its use in a wide range of *in vitro* preclinical models and, depending on the specific probe, may be multiplexed with other assays. However, there is a lack of understanding about how the activity of motile cilia, key cells in the respiratory tract, are linked to levels of NADH and FAD.

Role of motile cilia in respiratory medicine

Normal and effective ciliary activity is a critical component of respiratory system's defense against external agents. Impairment in ciliary activity and mucociliary clearance have been shown to be linked to the pathogenesis of many chronic and acute respiratory disease[25]. Ciliary activity has also been shown to impact the effectiveness of drug delivery to the respiratory system, especially for aerosolized compounds[42,43]. Therefore, compounds that stimulate ciliary activity may improve the outcome of respiratory diseases linked to impaired ciliary function.[25,44] Improving our understanding ciliary activity in the context of drug delivery requires understanding the dynamics of mucociliary clearance and ciliary activity, and how these cells responds to drugs

and drug delivery methods. Because of the role of cilia in the respiratory system, it is vital that microscopy assays designed for complex 3D models of the respiratory system can assess ciliary function. Optical coherence tomography is a potential optical modality that could be integrated with OMI to give a comprehensive understanding of cellular metabolism and ciliary activity in respiratory models.

Optical coherence tomography of ciliary activity

Optical coherence tomography (OCT) uses broadband coherent light to non-destructively visualize three-dimensional structural features in tissue at micrometer resolution with depths of up to 2mm. Contrast results from the extreme sensitivity of OCT to inhomogeneities in the refractive index of tissue resulting in elastic light scattering. Backscattered light from the sample is recombined with a reference beam causing an interference pattern related to the structure of the tissue through the inverse Fourier transform[45]. OCT is extremely versatile, and a wide range of functional extension have allowed OCT to image blood flow, vascular morphology, and tissue microstructure without the use of labels or dyes[46,47]. OCT has been especially successful in imaging motile cilia because it can quantify multiple parameters of ciliary motility in either 2D or 3D[48]. Cilia-driven fluid flow can be assessed with OCT using particle tracking velocimetry (PTV) where tracer particles, usually polystyrene beads, are sparsely seeded in the field-of-view and their center-of-mass is tracked across repeated frames to extract the in-plane velocity components[49]. Ciliary beat frequency (CBF) can be extracted from repeated frames by analyzing the time evolution of the speckle inherent to all OCT images[50,51]. Recent advances in OCT technology have also enabled the imaging of additional relevant respiratory structures, such as airway smooth muscle, and functional parameters, such as mucus viscoelasticity[52,53]. Overall, OCT is an

extremely versatile tool for imaging the respiratory system, and may offer complementary information to OMI for respiratory drug development assays.

CHAPTER II

MANUSCRIPT: ASSESSING TRACHEAL HEALTH USING OPTICAL METABOLIC IMAGING AND OPTICAL COHERENCE TOMOGRAPHY

Introduction

The health and pathophysiology of the tracheal mucosa is an important yet incompletely understood aspect of respiratory medicine. The tracheal mucosa is lined with cilia, hair-like organelles important for mucociliary clearance[48]. While the mechanisms of ciliary motility are not completely understood, dysfunction of ciliary motility, such as in primary ciliary dyskinesia and cystic fibrosis, is known to lead to severe disease phenotypes[25]. Optical techniques have allowed the investigation of fluid flow caused by the beating of motile cilia, and optical coherence tomography (OCT), a cross-sectional imaging technique, has been especially successful in imaging motile cilia because it can quantify multiple parameters of ciliary motility in either 2D or 3D[48]. Cilia-driven fluid flow can be assessed with OCT using particle tracking velocimetry (PTV) where tracer particles, usually polystyrene beads, are sparsely seeded in the field-of-view and their center-of-mass is tracked across repeated frames to extract the in-plane velocity components[49]. Ciliary beat frequency (CBF) can be extracted from repeated frames by analyzing the time evolution of the speckle inherent to all OCT images[50,51]. Recent advances in OCT technology have also enabled the imaging of additional relevant respiratory structures, such as airway smooth muscle, and functional parameters, such as mucus viscoelasticity[52,53].

However, OCT inherently lacks information about the molecular or biochemical state of cells. This is especially important because of the ATP-dependent nature of ciliary motor proteins[24]. Optical metabolic imaging (OMI) is an imaging technique that can quantitatively assess the metabolic state of cells by measuring the fluorescence intensities of endogenous metabolic co-

enzymes nicotinamide dinucleotide (NADH) and flavin adenine dinucleotide (FAD). By calculating the optical redox ratio (the intensity of NADH divided by the intensity of FAD), OMI is sensitive to the relative amounts of electron donors and acceptors within a cell. OMI is especially attractive for assessing tracheal health because OMI is label-free and ciliary function is tightly linked to the level of ATP coupled to NADH and FAD levels through multiple metabolic pathways[54]. OMI has had recent success in cancer biology, but the potential of OMI as a tool in assessing tracheal mucosal health and pathophysiology is unexplored[37,39].

Here, we present the results of a pilot study investigating the potential utility of OMI to assess the status of tracheal mucosal health. We studied well-established, quantitative, endogenous contrast-based OMI measures in *ex vivo* mouse trachea using widefield epifluorescence microscopy and compared these to OCT endpoints. We established normative values in healthy trachea as well as perturbed values in the setting of metabolic disruption using sodium cyanide.

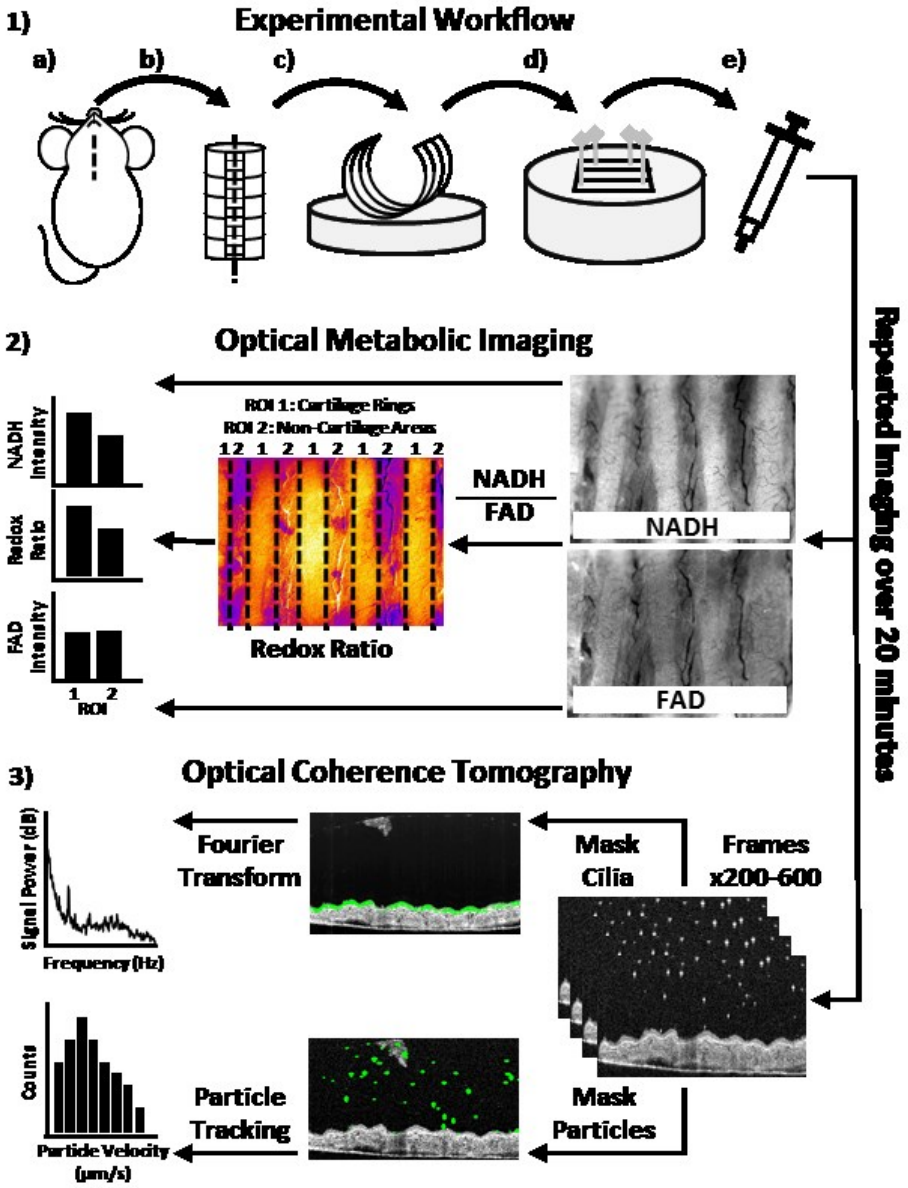

Figure 1. Experimental Workflow. 1) a) After euthanasia, a midline incision was made and the trachea was dissected from surrounding tissue. b) After the trachea was removed, the trachealis muscle was cut to expose the mucosal surface. c) The trachea was then rinsed in DMEM media. d) For imaging, the trachea was pinned down to PDMS lining the bottom of a 35mm dish. e) After baseline imaging, each trachea was treated with 10mM sodium cyanide. **2)** Optical metabolic imaging is performed by acquiring an NADH fluorescence intensity image and an FAD fluorescence intensity image. The redox ratio is calculated by dividing the NADH intensity image by FAD intensity image. Two regions-of-interest are then defined to separate regions with cartilage rings (ROI 1) and regions without cartilage (ROI 2). **2)** Optical coherence tomography imaging of cilia beat frequency and particle velocity is performed by taking repeated B-scans at a single location. To extract the cilia beat frequency spectrum, pixels containing cilia are first masked and the spectra of these pixels are averaged to yield a CBF spectrum for each time point. For particle tracking velocimetry, the particles are first masked and tracked over multiple frames using TrackMate[55].

Methods

Ex vivo murine trachea preparation

All animal work was approved by the Vanderbilt University's Institution Animal Care and Use Committee. Wild-type mice (female, 6-8 weeks, FVB/NJ, The Jackson Laboratory) were euthanized by exsanguination under isoflurane anesthesia and a midline incision was made to expose the trachea (Fig 1.1a). Surrounding tissue, including the esophagus, was bluntly dissected away and the entire trachea was removed by cutting below the larynx and above the lungs with scissors (Fig 1.1b). The trachea was placed immediately into a 35mm dish filled with DMEM/F12 media (Fisher Scientific), and Vannas micro scissors (Fine Science Tools) were used to cut along the trachealis muscle to expose the mucosal surface (Fig 1.1c). Lastly, the trachea was transferred into a 35mm dish lined with cured polydimethylsiloxane (PDMS, Quantum Silicones), pinned with the mucosal surface of the trachea facing the top of the dish, and covered with warmed (37°C) DMEM/F12 media (FisherScientific) (Fig 1.1d). The dish was placed in a stage top incubator during imaging to maintain physiological temperatures. For each trachea, baseline imaging was first performed using either OMI or OCT. The media was then changed and the trachea was covered with warmed (37°C) DMEM/F12 media containing 10mM sodium cyanide (Sigma) (Fig 1.1e). Repeated imaging then was performed over 20 minutes with time points every 2 minutes (Fig 1.2 & Fig 1.3).

Widefield optical metabolic imaging instrumentation and image analysis

Ex vivo mouse tracheae (n=5) were imaged using an upright epifluorescence microscope (Nikon Ni-U) using a 4x air objective (Nikon CFI Plan Fluor, NA 0.13, FOV: 1.65mm x 2.2mm), a white light LED source (X-Cite 120LED), and an interline CCD (Andor Clara E) thermoelectrically

cooled to -20°C. NADH fluorescence was excited (power at 375nm: 1.6mW) and integrated over 2s using a DAPI filter cube (Nikon, ex: 361-389nm/em: 435-485nm) and FAD fluorescence was excited (power at 450nm: 1.27mW) and integrated over 6s using a GFP filter cube (Nikon, ex: 450-490nm/em: 500-550nm). Redox ratio images were calculated by dividing the intensity of NADH by the intensity of FAD for each pixel within the field of view (ImageJ). Because the trachea consists of interrupted rings of tracheal cartilage, two regions-of-interest (ROI 1: Cartilage rings, ROI 2: Non-cartilage areas) were selected for each NADH, FAD, and redox ratio image and the mean value was calculated for each ROI from each image. Sodium cyanide has no known visible fluorescence or absorption optical properties. A control experiment with no sodium cyanide treatment showed no significant change in redox ratio due to photobleaching or phototoxicity over 20 minutes caused by widefield OMI (data not shown).

Optical coherence tomography instrumentation

All OCT measurements were performed on *ex vivo* mouse tracheae (CBF analysis: n=1, PTV: n=1) with a commercial OCT system (Thorlabs Telesto II) with a center wavelength of 1300nm, axial resolution of 5.5μm in air ($\Delta\lambda$ = 170nm), and a lateral resolution of 13μm (Thorlabs OCT-LK3). Each B-scan was composed of 600 pixels scanned over 3.0mm (5μm/pixel) laterally and 1024 pixels axially over 3.5mm in air (3.4μm/pixel).

Ciliary beat frequency spectral analysis

For CBF spectral measurements, 600 repeated B-scans were acquired with an A-scan rate of 48kHz resulting in an effective B-scan rate of 52Hz and a maximum detectable CBF of 26Hz. An algorithm written in MATLAB (MathWorks) was used to calculate the CBF spectrum from the periodic fluctuation of each pixel's intensity speckle pattern. A Fourier transform of each pixel

across the 600 repeated B-scans in the time domain (zero-padded to 2048) yielded the CBF power spectrum. To analyze only pixels that contain beating cilia, the per-pixel speckle variance was calculated across the repeated B-scans. Regions of the highest variance were segmented based on Otsu's thresholding and the power spectra of only these pixels were averaged to yield the CBF power spectrum for each time point[56]. The spectral region of 20-26Hz was excluded from further analysis because of high noise power and the knowledge of typical CBF values between 5-15Hz[24]. CBF power spectra were calculated for every OCT time point. To quantify overall changes in spectral power, the area under the curve of each CBF power spectrum was integrated between 4-10Hz. This fully-automated analysis was performed in less than 20s per time point on a desktop computer (Dell, Intel Xeon E5-1603 2.8GHz, 64.0GB, 64-bit Windows 10). Future control experiment with no sodium cyanide treatment will be performed to show the repeatability of the CBF power spectrum measurement.

Particle tracking velocimetry

For PTV measurements, a 10% suspension of 10μm polystyrene beads (Bangs Laboratories PS07N) was diluted with DMEM media for a final volume percent of 0.2% beads/media. Approximately 2μL of the final suspension was added to the media already covering the trachea yielding 20-30 beads per field-of-view. Because these beads settle on the mucosal surface of the trachea and may interfere with ciliary beating, PTV was only performed at baseline and 20 minutes after sodium cyanide treatment. PTV was performed using the ImageJ/FIJI plugin TrackMate[55]. Briefly, each particle's center-of-mass was detected using the difference of Gaussians method and tracked across 8 frames (1Hz) using the linear motion tracker, which uses a Kalman filter to predict each particle's future location based on Bayesian statistics. The data for each tracked particle was then exported to MATLAB for further analysis. Future control experiments will be performed to

ensure that any change in ciliary beating is due to a response to sodium cyanide, and not caused by polystyrene bead settling.

Statistics

To assess the effect of sodium cyanide treatment, the mean and 95% confidence interval was calculated for each endpoint with more than one sample. Student's t-tests at every time point were also performed, with the significance level corrected for multiple comparisons using Bonferroni's correction. Statistical significance is indicated with * for $p<0.05$.

Results

Redox ratio is sensitive to sodium cyanide treatment

The metabolism of *ex vivo* mouse tracheae was perturbed with 10mM sodium cyanide. Cyanide is a known inhibitor of oxidative phosphorylation, which when blocked leads to an overabundance of NADH in the cytoplasm. Figure 2.1 shows representative images of NADH fluorescence, FAD fluorescence and redox ratio before and after cyanide treatment. Qualitatively, these images show the increase in redox ratio and NADH fluorescence intensity due to cyanide treatment. Morphologically, the trachea consists of two regions: ROI 1: areas containing cartilage rings, and ROI 2: areas with no cartilage. Rather than integrating over the entire field of view, these two regions were segmented and analyzed separately.

When the OMI images were quantified over time, both regions-of-interest showed significant increases in redox ratio ($p<0.05$). The regions with cartilage (ROI1) had a larger increase of 55% (95% CI: [32% 79%]) compared to 38% in regions without cartilage (95% CI: [12% 63%]) (Fig 2.2). This was driven by an initial increase in NADH fluorescence intensity (ROI 1: 14%, 95% CI: [-5% 14%], ROI 2: 16%, 95% CI: [3% 27%]) that continued to increase with the

maximum achieved at 16 minutes (ROI 1: 36% 95% CI: [-1% 75%], ROI 2: 23%, 95% CI: [1% 44%]) (Fig 2.2). The increase in redox ratio was also driven by a decrease in FAD fluorescence intensity, with its minimum at 20 minutes (ROI 1: -13% 95% CI: [-29% 7%], ROI 2: -13%, 95% CI: [-25% 7%]) (Fig 2.2).

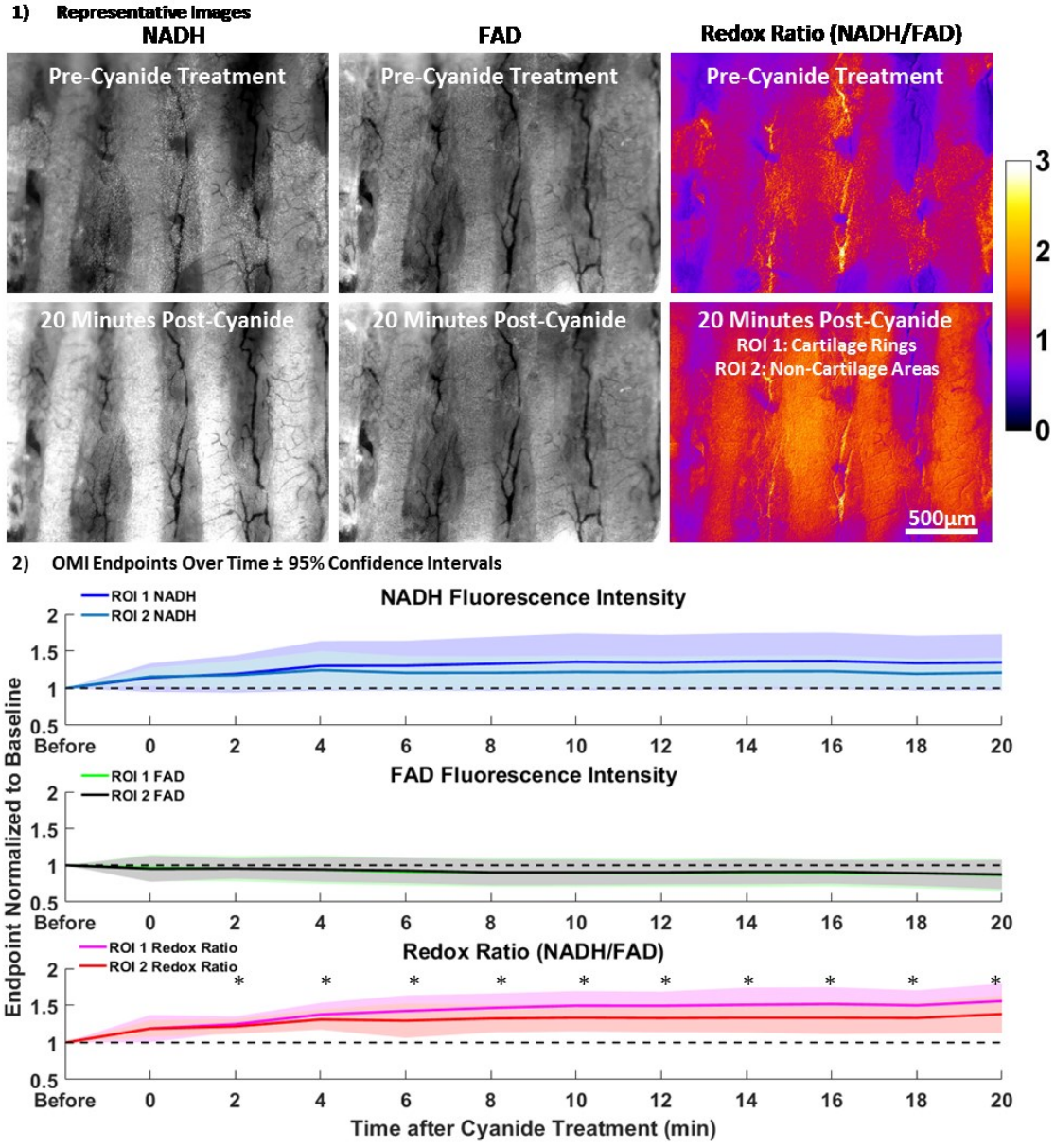

Figure 2. Optical Metabolic Imaging of the Trachea. 1) Representative images show NADH fluorescence intensity, FAD fluorescence intensity, and the redox ratio (NADH/FAD) both before sodium cyanide treatment and 20 minutes after sodium cyanide treatment. To quantify these images, two regions-of-interest were defined to separate regions with cartilage rings (ROI 1) and regions without cartilage (ROI 2). **2)** Graph of OMI endpoints (NADH intensity, FAD intensity,

and redox ratio) normalized to baseline shows that sodium cyanide leads to a statistically significant increase in redox ratio, driven by an increase in NADH fluorescence and slight decrease in FAD fluorescence. Both regions-of-interest show an increase in redox ratio (ROI 1: 55%, 95% CI: [32% 79%], ROI 2: 38%, 95% CI: [12% 63%]). Statistical significance indicated with * for $p<0.05$.

Sodium cyanide reduces ciliary activity

The trachea is lined with ciliated epithelial cells that beat to move mucus away from the lungs. Ciliary beating continues when the trachea is removed and placed in media at 37°C. Two complementary methods (CBF spectral analysis and PTV) were used to assess the effect of sodium cyanide on ciliary activity. Although the spatial resolution of the OCT system is insufficient to fully resolve the structure of the cilia, ciliary beating causes oscillations in the OCT intensity speckle allowing analysis of the CBF spectrum. To analyze only pixels containing cilia, a mask was created by calculating the speckle variance across 600 repeated frames and thresholding for the pixels with highest variance (Fig 3.1). Because variance is proportional to the power spectral density through Parseval's theorem, pixels with high variance represent pixels with high power in the frequency band bounded by the spectral resolution (0.1Hz) and Nyquist frequency (26Hz)[50]. This method robustly selected pixels on the mucosal surface for every time point. The CBF spectra averaged across all masked pixels show a distinct peak at 5.9Hz that is fully ablated 20 minutes after treatment with 10mM sodium cyanide (Fig 3.2). Calculating the area-under-the-curve (AUC) of the CBF power spectra results in a bulk measure of the overall changes in spectral power between each time point and baseline. The AUC shows an initial increase in spectral power (indicating an overall increase in the CBF power spectrum) followed by a decline in spectral power (indicating an increase in the overall CBF power spectrum) by 20 minutes after cyanide treatment. Additional control studies with no sodium cyanide treatment are planned to understand the repeatability and reliability of the CBF power spectrum measurement.

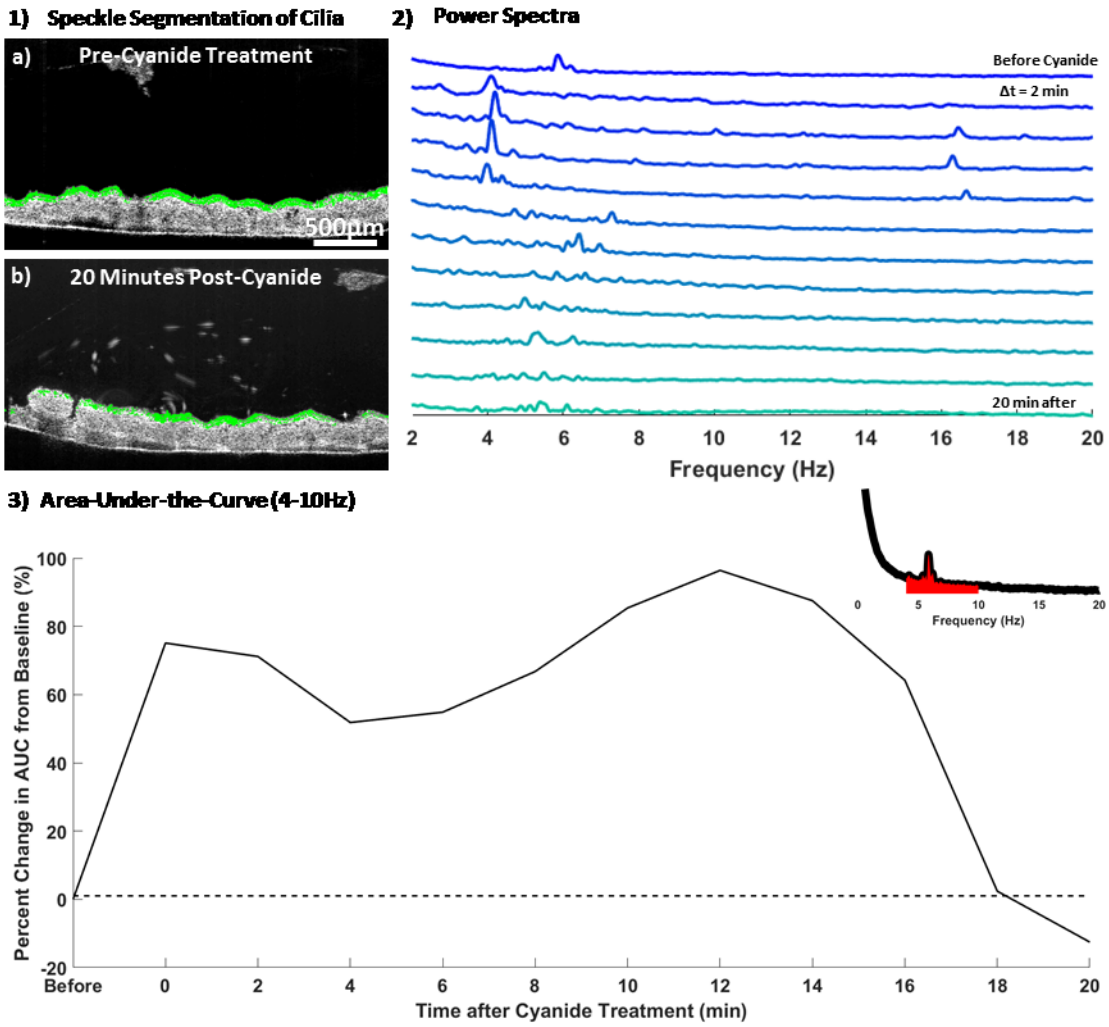

Figure 3. Ciliary Beat Frequency Spectral Analysis. 1) Regions with high speckle variance were used as a mask to include the CBF spectra from pixels with beating cilia. **2)** The CBF power spectra show an initial peak at 6.8Hz that is eliminated 20 minutes after sodium cyanide treatment. Each spectrum is acquired at 2 minute intervals. **3)** The area-under-the-curve of the 4-10Hz spectral range shows an initial increase in spectral power followed by a decline in spectral power by 20 minutes after sodium cyanide treatment.

PTV measures cilia-driven fluid flow by tracking the transport of polystyrene microbeads suspended in media above the cilia, with reduction in particle velocity indicative of a reduction in ciliary activity. Maximum intensity projections over 200 frames (23Hz) qualitatively shows that particle velocity is reduced by sodium cyanide treatment (Fig 4.1a & Fig 4.1.b). To quantify this data, particles were tracked over 8 frames (1Hz) using TrackMate and these data show that the

median particle velocity is reduced (Before: 10.88μm/s, After: 4.22μm/s) and particle velocity histogram is shifted towards zero by sodium cyanide treatment (Fig 4.2)[55].

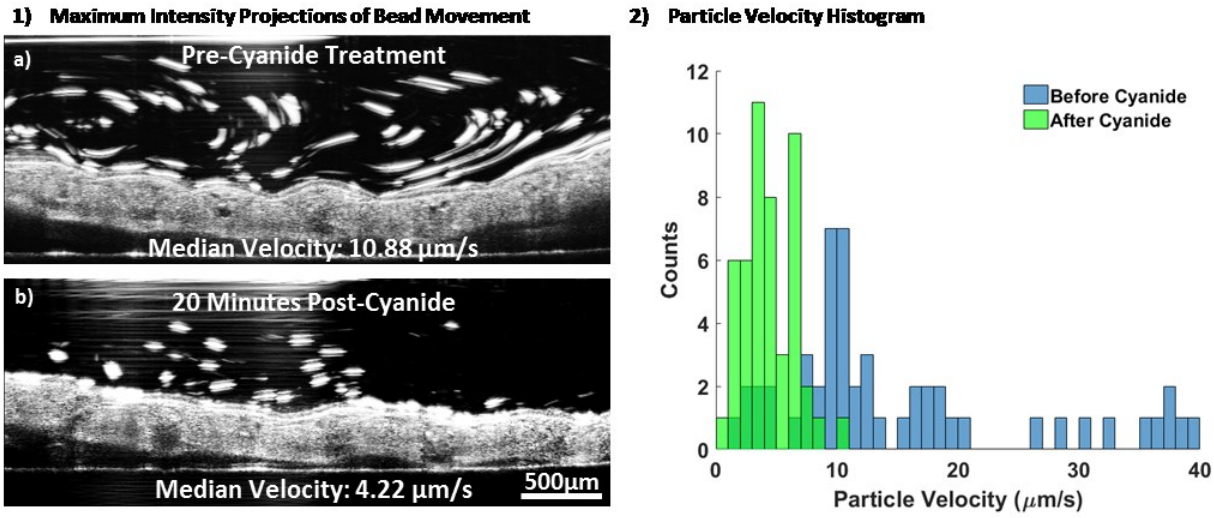

Figure 4. Particle Tracking Velocimetry. 1) Maximum intensity projections over 200 frames (23Hz) qualitatively shows that particle velocity is reduced by sodium cyanide treatment. **2)** Particle tracking velocimetry over 8 frames (1Hz) using TrackMate quantitatively shows that the median particle velocity is reduced (Before: 10.88μm/s, After: 4.22μm/s) and particle velocity histogram is shifted towards zero by sodium cyanide treatment[55].

Discussion

The respiratory epithelium is lined with cilia that must effectively beat together to clear mucus, pathogens, and toxins from the lungs through mucociliary clearance. While significant dysfunction is known to cause severe disease phenotypes, the complex mechanisms that modulate ciliary function are not completely understood[25,57]. Specifically, it is unclear if subtle variation in ciliary activity underlie changes in the severity of inflammatory respiratory diseases such as chronic obstructive pulmonary disease and asthma. OCT has been demonstrated as a versatile technique that can effectively monitor multiple parameters of ciliary function[48]. However, OCT inherently lacks molecular and biochemical information about the drivers of ciliary activity and information about other cells in the tracheal mucosa. OMI is a complementary technique to OCT because it can assess changes in cellular metabolism in both cilia and other constituent cells in the

trachea, and has been shown to sensitive to a cell's microenvironment, toxicity of drugs, cellular phenotype, and the spatial distribution of cells[37,40].

In this study, we demonstrated the feasibility of performing widefield OMI and OCT on intact mouse trachea to acquire metabolic and functional information across multiple cell types. Autofluorescence images of NADH and FAD, as well as calculated redox ratio images, revealed the metabolic response of the tracheal mucosa to sodium cyanide. Cyanide lead to an increase in NADH fluorescence and decrease in FAD fluorescence that drove a statistically significant increase in the redox ratio. Because OMI yields 2D images, two distinct tracheal regions were identified with regions containing cartilage under the epithelium showed larger increases in redox ratio compared to the rest of the trachea, which may be because of larger numbers of metabolically active cells, specifically chondrocytes, in the cartilage responding to cyanide treatment. Control experiments also showed that repeated OMI did not change the redox ratio significantly, showing that photobleaching

OCT also resolved the inhibitor effect of sodium cyanide on ciliary activity by assessing ciliary activity through the CBF, specifically that spectral power of the CBF power spectrum between 4-10Hz was decreased 20 minutes after cyanide treatment. While both the axial and lateral resolution of our OCT system (4.1μm in water and 13 μm, respectively) was too low to individually resolve each cilium (approximately 1-10μm in length and 1 μm in width) according to Nyquist sampling requirements, analyzing OCT speckle makes it is possible to resolve the sub-resolution dynamics of cell movement – the principle of angiographic OCT methods[46]. Because cilia are known to beat in metachronal waves, the speckle from a specific pixel therefore likely represents the coherent ensemble of many cilia beating at the same frequency with constant phase differences between each cilium[24]. Our fully-automated CBF analysis was compared to cilia-driven fluid flow

assessed with PTV of polystyrene microbeads, a more established method of evaluating ciliary motility that serves as validation of our approach[48]. Because of the small sample size of tracheae used for the OCT studies, statistical analysis could not be performed, but these preliminary studies potentially indicate a biphasic response to sodium cyanide. Overall, these results agree with the known mechanism of sodium cyanide, which is to block oxidative phosphorylation by inhibiting complex III activity. In addition to sodium cyanide treatment being a proof-of-concept demonstration, many bacterial species produce hydrogen cyanide, specifically *Pseudomonas aeruginosa* and *Streptococcus aureas*, both important causes of morbidity and mortality in cystic fibrosis and acute respiratory infection[58,59].

These results suggest the feasibility of OMI for evaluating the metabolism of multiple cell types in and regions of the trachea without the need for exogenous dyes or destructive histology. This method could be used not only preclinically to study the effects of novel therapies on subtypes of tracheal cells in mice, but also in critical care medicine for monitoring patient tracheal health and preventing respiratory infection.

CHAPTER III

CONCLUSIONS AND FUTURE DIRECTION

The metabolic response of the tracheal mucosa to sodium cyanide was evaluated using optical metabolic imaging combined with optical coherence tomography. Treatment with sodium cyanide significantly increased the redox ratio due to an increase in NADH fluorescence intensity and a slight decrease in FAD intensity, agreeing with the known effect of sodium cyanide as an inhibitor of oxidative phosphorylation. The response of different cellular populations of cells including epithelial cells and chondrocytes was resolved. Optical coherence tomography resolved decreases in ciliary activity from sodium cyanide treatment, which was expected due to the reliance of cilia on oxidative phosphorylation. Overall, our multimodal approach offers complementary data about the health of cells in the trachea, which may provide a new tool for preclinical research and *in vivo* patient monitoring.

Possible future directions for this technology include applications in respiratory drug development and basic science. A vital component of drug development is to understand the mechanism of action and cytotoxic potential of new therapeutics, but most assays were designed for cell monolayers and integrate a response over an entire population of cells and require the sacrifice of cells at each time point. Specifically, there is an unmet need for new cytotoxicity assays that can non-invasively monitor organomimetic cultures over multiple days. OCT is widely used as a volumetric imaging technique and therefore would be compatible with advance 3D cultures, but our OMI approach based on epifluorescence microscopy does not yield 3D images. To be applicable in 3D cultures, OMI must be able to optically section through a sample. OMI has been successfully performed using two-photon fluorescence microscopy, yielding optical sections with low phototoxicity due to the physics of two-photon fluorescence excitation, but requires expensive

femtosecond near-infrared lasers. Two other potential approaches based on single-photon fluorescence include confocal fluorescence microscopy and structured illumination optical sectioning microscopy that can both be implemented with simpler illumination sources such as lamps or light-emitting diodes and achieve optical sectioning through a confocal pinhole or spatial modulation of the illumination projected on the sample, but this approach may cause phototoxicity. Future studies are required to understand if single-photon OMI causes significant phototoxicity that may confound results of drug response and cytotoxicity studies. Our results suggest that development of rapid OMI with optical sectioning would allow the multimodal approach of OMI and OCT to be better applied to advanced cultures for cytotoxicity screening.

In terms of understanding drug mechanism of action and for basic science studies, our imaging platform applied to *ex vivo* tissue would allow the study of the interaction of compounds, toxins, nanoparticles, bacteria, and viruses with the tracheal mucosa, respiratory epithelium, and airway smooth muscle that would improve our understanding of respiratory disease pathogenesis. Human tracheal tissue can be acquired from explant lungs, providing a highly relevant tissue source for these studies. The first proposed study is to explore the link between NADH and FAD levels and ciliary activity using acute biochemical and metabolic perturbations such as ATP, acetylcholine, LPS (as a model of sepsis), 2DG (glycolysis inhibitor), rotenone (complex I inhibitor), hyperoxia/hypoxia, and pyocyanin (excretion of *P. aeruginosa)*. Then, co-cultures of trachea and relevant bacteria such as *P. aeruginosa* and *S. aureus* with and without antibiotics could be used to explore the mechanisms of bacterial infection in the respiratory system and identify new targets for novel antibiotics. Overall, this technology merits future development due to its potential applications in both drug development and basic science.

REFERENCES

1. Ferkol T, Schraufnagel D. The Global Burden of Respiratory Disease. *Ann Am Thorac Soc*. 2014;11(3):404-406. doi:10.1513/AnnalsATS.201311-405PS.

2. Wang H, Naghavi M, Allen C, et al. Global, regional, and national life expectancy, all-cause mortality, and cause-specific mortality for 249 causes of death, 1980–2015: a systematic analysis for the Global Burden of Disease Study 2015. *Lancet*. 2016;388(10053):1459-1544. doi:10.1016/S0140-6736(16)31012-1.

3. Vos T, Allen C, Arora M, et al. Global, regional, and national incidence, prevalence, and years lived with disability for 310 diseases and injuries, 1990–2015: a systematic analysis for the Global Burden of Disease Study 2015. *Lancet*. 2016;388(10053):1545-1602. doi:10.1016/S0140-6736(16)31678-6.

4. Schluger NW, Koppaka R. Lung Disease in a Global Context. A Call for Public Health Action. *Ann Am Thorac Soc*. 2014;11(3):407-416. doi:10.1513/AnnalsATS.201312-420PS.

5. Roche N. Where current pharmacological therapies fall short in COPD: symptom control is not enough. *Eur Respir Rev*. 2007;16(105).

6. Barnes PJ. Severe asthma: advances in current management and future therapy. *J Allergy Clin Immunol*. 2012;129(1):48-59. doi:10.1016/j.jaci.2011.11.006.

7. WHO | Global tuberculosis report 2016. *WHO*. 2016.

8. WHO | Ending preventable child deaths from pneumonia and diarrhoea by 2025. *WHO*. 2013.

9. Günther G, Gunther G, Günther G. Multidrug-resistant and extensively drug-resistant tuberculosis: a review of current concepts and future challenges. *Clin Med*. 2014;14(3):279-285. doi:10.7861/clinmedicine.14-3-279.\

10. Karchmer AW. Increased antibiotic resistance in respiratory tract pathogens: PROTEKT US--an update. *Clin Infect Dis*. 2004;39 Suppl 3(Supplement 3):S142-50. doi:10.1086/421352.

11. Barnes PJ, Bonini S, Seeger W, Belvisi MG, Ward B, Holmes A. Barriers to new drug development in respiratory disease. *Eur Respir J*. 2015;45(5):1197-1207. doi:10.1183/09031936.00007915.

12. DiMasi JA, Grabowski HG, Hansen RW. Innovation in the pharmaceutical industry: New estimates of R&D costs. *J Health Econ*. 2016;47:20-33. doi:10.1016/j.jhealeco.2016.01.012.

13. Aryan E, Makvandi M, Farajzadeh A, et al. Clinical value of IS6110-based loop-mediated isothermal amplification for detection of Mycobacterium tuberculosis complex in respiratory specimens. *J Infect*. 2013;66(6):487-493. doi:10.1016/j.jinf.2013.02.005.

14. Bhattacharya S, Zhang Q, Carmichael PL, Boekelheide K, Andersen ME. Toxicity Testing in the 21st Century: Defining New Risk Assessment Approaches Based on Perturbation of Intracellular Toxicity Pathways. Zhang B, ed. *PLoS One*. 2011;6(6):e20887. doi:10.1371/journal.pone.0020887.

15. Shanks N, Greek R, Greek J. Are animal models predictive for humans? *Philos Ethics, Humanit Med*. 2009;4(1):2. doi:10.1186/1747-5341-4-2.

16. Sun H, Xia M, Austin CP, Huang R. Paradigm Shift in Toxicity Testing and Modeling. *AAPS J*. 2012;14(3):473-480. doi:10.1208/s12248-012-9358-1.

17. Maltman DJ, Przyborski SA. Developments in three-dimensional cell culture technology aimed at improving the accuracy of *in vitro* analyses. *Biochem Soc Trans*. 2010;38(4):1072-1075. doi:10.1042/BST0381072.

18. Stennert E, Siefer O, Zheng M, Walger M, Mickenhagen A. In vitro culturing of porcine tracheal mucosa as an ideal model for investigating the influence of drugs on human respiratory mucosa. *Eur Arch Otorhinolaryngol*. 2008;265(9):1075-1081. doi:10.1007/s00405-008-0661-5.

19. Huh D, Leslie DC, Matthews BD, et al. A Human Disease Model of Drug Toxicity-Induced Pulmonary Edema in a Lung-on-a-Chip Microdevice. *Sci Transl Med*. 2012;4(159):159ra147-159ra147. doi:10.1126/scitranslmed.3004249.

20. Nichols JE, Niles JA, Vega SP, Cortiella J. Novel in vitro respiratory models to study lung development, physiology, pathology and toxicology. *Stem Cell Res Ther*. 2013;4(Suppl 1):S7. doi:10.1186/scrt368.

21. Huh D, Matthews BD, Mammoto A, Montoya-Zavala M, Hsin HY, Ingber DE. Reconstituting Organ-Level Lung Functions on a Chip. *Science (80-)*. 2010;328(5986).

22. O'Brien PJ. High-Content Analysis in Toxicology: Screening Substances for Human Toxicity Potential, Elucidating Subcellular Mechanisms and *In Vivo* Use as Translational Safety Biomarkers. *Basic Clin Pharmacol Toxicol*. 2014;115(1):4-17. doi:10.1111/bcpt.12227.

23. McKim JM, Jr. Building a tiered approach to in vitro predictive toxicity screening: a focus on assays with in vivo relevance. *Comb Chem High Throughput Screen*. 2010;13(2):188-206. doi:10.2174/138620710790596736.

24. Satir P, Christensen ST. Overview of structure and function of mammalian cilia. *Annu Rev Physiol*. 2007;69:377-400. doi:10.1146/annurev.physiol.69.040705.141236.

25. Tilley AE, Walters MS, Shaykhiev R, Crystal RG. Cilia Dysfunction in Lung Disease. *Annu Rev Physiol*. 2015;77(1):379-406. doi:10.1146/annurev-physiol-021014-071931.

26. Barnes PJ. Immunology of asthma and chronic obstructive pulmonary disease. *Nat Rev Immunol*. 2008;8(3):183-192. doi:10.1038/nri2254.

27. Benam KH, Dauth S, Hassell B, et al. Engineered In Vitro Disease Models. *Annu Rev Pathol Mech Dis*. 2015;10(1):195-262. doi:10.1146/annurev-pathol-012414-040418.

28. O'Brien PJ. Discovery Toxicology Screening: Predictive,In Vitro Cytotoxicity. In: Wiley-VCH Verlag GmbH & Co. KGaA; :323-343. doi:10.1002/9783527627448.ch14.

29. Fotakis G, Timbrell JA. In vitro cytotoxicity assays: comparison of LDH, neutral red, MTT and protein assay in hepatoma cell lines following exposure to cadmium chloride. *Toxicol Lett*. 2006;160(2):171-177. doi:10.1016/j.toxlet.2005.07.001.

30. van Tonder A, Joubert AM, Cromarty AD. Limitations of the 3-(4,5-dimethylthiazol-2-yl)-2,5-diphenyl-2H-tetrazolium bromide (MTT) assay when compared to three commonly used cell enumeration assays. *BMC Res Notes*. 2015;8:47. doi:10.1186/s13104-015-1000-8.

31. Faller B, Urban L. *Hit and Lead Profiling : Identification and Optimization of Drug-like Molecules*. Wiley-VCH; 2009.

32. Kühn J, Shaffer E, Mena J, et al. Label-free cytotoxicity screening assay by digital holographic microscopy. *Assay Drug Dev Technol*. 2013;11(2):101-107. doi:10.1089/adt.2012.476.

33. Tseng H, Gage JA, Shen T, et al. A spheroid toxicity assay using magnetic 3D bioprinting and real-time mobile device-based imaging. *Sci Rep*. 2015;5:13987. doi:10.1038/srep13987.

34. Moczko E, Mirkes EM, Cáceres C, et al. Fluorescence-based assay as a new screening tool for toxic chemicals. *Sci Rep*. 2016;6:33922. doi:10.1038/srep33922.

35. Hynes J, Carey C, Will Y. Fluorescence-Based Microplate Assays for In Vitro Assessment of Mitochondrial Toxicity, Metabolic Perturbation, and Cellular Oxygenation. In: *Current Protocols in Toxicology*. Hoboken, NJ, USA: John Wiley & Sons, Inc.; 2016:2.16.1-2.16.30. doi:10.1002/cptx.3.

36. Dykens JA, Will Y. The significance of mitochondrial toxicity testing in drug development. *Drug Discov Today*. 2007;12(17):777-785. doi:10.1016/j.drudis.2007.07.013.

37. Walsh AJ, Cook RS, Sanders ME, et al. Quantitative optical imaging of primary tumor organoid metabolism predicts drug response in breast cancer. *Cancer Res*.

2014;74(18):5184-5194. doi:10.1158/0008-5472.CAN-14-0663.

38. Sharick JT, Gil DA, Choma MA, Skala MC. Optical metabolic imaging for monitoring tracheal health. In: Farkas DL, Nicolau D V., Leif RC, eds. International Society for Optics and Photonics; 2016:971108. doi:10.1117/12.2212779.

39. Skala MC, Riching KM, Gendron-Fitzpatrick A, et al. In vivo multiphoton microscopy of NADH and FAD redox states, fluorescence lifetimes, and cellular morphology in precancerous epithelia. *Proc Natl Acad Sci*. 2007;104(49):19494-19499. doi:10.1073/pnas.0708425104.

40. Shah AT, Diggins KE, Walsh AJ, Irish JM, Skala MC. In Vivo Autofluorescence Imaging of Tumor Heterogeneity in Response to Treatment. *Neoplasia*. 2015;17(12):862-870. doi:10.1016/j.neo.2015.11.006.

41. CHANCE B, LEGALLAIS V, SCHOENER B. Metabolically linked changes in fluorescence emission spectra of cortex of rat brain, kidney and adrenal gland. *Nature*. 1962;195:1073-1075. http://www.ncbi.nlm.nih.gov/pubmed/13878020. Accessed November 7, 2016.

42. Steimer A, Haltner E, Lehr C-M. Cell Culture Models of the Respiratory Tract Relevant to Pulmonary Drug Delivery. *J Aerosol Med*. 2005;18(2):137-182. doi:10.1089/jam.2005.18.137.

43. Gizurarson S. The Effect of Cilia and the Mucociliary Clearance on Successful Drug Delivery. *Biol Pharm Bull*. 2015;38(4):497-506. doi:10.1248/bpb.b14-00398.

44. Sears PR, Thompson K, Knowles MR, Davis CW. Human airway ciliary dynamics. *AJP Lung Cell Mol Physiol*. 2013;304(3):L170-L183. doi:10.1152/ajplung.00105.2012.

45. Izatt JA, Choma MA. Theory of Optical Coherence Tomography. In: Springer Berlin Heidelberg; 2008:47-72. doi:10.1007/978-3-540-77550-8_2.

46. Mariampillai A, Standish BA, Moriyama EH, et al. Speckle variance detection of microvasculature using swept-source optical coherence tomography. *Opt Lett*. 2008;33(13):1530. doi:10.1364/OL.33.001530.

47. Vermeer KA, Mo J, Weda JJA, Lemij HG, de Boer JF. Depth-resolved model-based reconstruction of attenuation coefficients in optical coherence tomography. *Biomed Opt Express*. 2013;5(1):322-337. doi:10.1364/BOE.5.000322.

48. Huang BK, Choma MA. Microscale imaging of cilia-driven fluid flow. *Cell Mol Life Sci*. 2015;72(6):1095-1113. doi:10.1007/s00018-014-1784-z.

49. Jonas S, Bhattacharya D, Khokha MK, Choma MA. Microfluidic characterization of cilia-driven fluid flow using optical coherence tomography-based particle tracking velocimetry.

Biomed Opt Express. 2011;2(7):2022-2034. doi:10.1364/BOE.2.002022.

50. Oldenburg AL, Chhetri RK, Hill DB, Button B. Monitoring airway mucus flow and ciliary activity with optical coherence tomography. *Biomed Opt Express*. 2012;3(9):1978-1992. doi:10.1364/BOE.3.001978.

51. Lemieux BT, Chen JJ, Jing J, Chen Z, Wong BJF. Measurement of ciliary beat frequency using Doppler optical coherence tomography. *Int Forum Allergy Rhinol*. 2015;0(0):n/a-n/a. doi:10.1002/alr.21582.

52. Chu KK, Mojahed D, Fernandez CM, et al. Particle-Tracking Microrheology Using Micro-Optical Coherence Tomography. *Biophys J*. 2016;111(5):1053-1063. doi:10.1016/j.bpj.2016.07.020.

53. Adams DC, Hariri LP, Miller AJ, et al. Birefringence microscopy platform for assessing airway smooth muscle structure and function in vivo. *Sci Transl Med*. 2016;8(359).

54. Alberts B, Johnson A, Lewis J, Raff M, Roberts K, Walter P. *Molecular Biology of the Cell, 6th Edition*.; 2015. doi:10.1002/bmb.20192.

55. Tinevez J-Y, Perry N, Schindelin J, et al. TrackMate: An open and extensible platform for single-particle tracking. *Methods*. doi:http://dx.doi.org/10.1016/j.ymeth.2016.09.016.

56. Otsu N. A Threshold Selection Method from Gray-Level Histograms. *IEEE Trans Syst Man Cybern*. 1979;9(1):62-66. doi:10.1109/TSMC.1979.4310076.

57. Gudis DA, Cohen NA. Cilia Dysfunction. *Otolaryngol Clin North Am*. 2010;43(3):461-472. doi:10.1016/j.otc.2010.02.007.

58. Neerincx AH, Linders YAM, Vermeulen L, et al. Hydrogen cyanide emission in the lung by *Staphylococcus aureus*. *Eur Respir J*. 2016;48(2):577-579. doi:10.1183/13993003.02093-2015.

59. Nair C, Shoemark A, Chan M, et al. Cyanide levels found in infected cystic fibrosis sputum inhibit airway ciliary function. *Eur Respir J*. 2014;44(5):1253-1261. doi:10.1183/09031936.00097014.